Atomistic Simulations of Functional Au144(SR)60 Gold Nanoparticles in Aqueous Environment

ARTICLE *in* THE JOURNAL OF PHYSICAL CHEMISTRY C · APRIL 2012

Impact Factor: 4.77 · DOI: 10.1021/jp301094m

THE JOURNAL OF PHYSICAL CHEMISTRY C

Article

pubs.acs.org/JPCC

Atomistic Simulations of Functional $Au_{144}(SR)_{60}$ Gold Nanoparticles in Aqueous Environment

Elena Heikkilä,[†] Andrey A. Gurtovenko,[‡,§] Hector Martinez-Seara,[†] Hannu Häkkinen,[∥] Ilpo Vattulainen,[†,⊥] and Jaakko Akola*[,†,∥,#]

[†]Department of Physics, Tampere University of Technology, P.O. Box 692, FI-33101 Tampere, Finland

[‡]Institute of Macromolecular Compounds, Russian Academy of Sciences, Bolshoi Prospect 31, V.O., St. Petersburg, 199004, Russia

[§]Department of Molecular Biophysics, Faculty of Physics, St. Petersburg State University, St. Petersburg, 198504, Russia

[∥]Departments of Physics and Chemistry, Nanoscience Center, University of Jyväskylä, FI-40014 Jyväskylä, Finland

[⊥]Center for Biomembrane Physics (MEMPHYS), University of Southern Denmark, Odense, DK-5230 Denmark

[#]Institut für Festkörperforschung, Forschungszentrum Jülich, D-52425 Jülich, Germany

Supporting Information

ABSTRACT: Charged monolayer-protected gold nanoparticles (AuNPs) have been studied in aqueous solution by performing atomistic molecular dynamics simulations at physiological temperature (310 K). Particular attention has been paid to electrostatic properties that modulate the formation of a complex comprised of the nanoparticle together with surrounding ions and water. We focus on Au_{144} nanoparticles that comprise a nearly spherical Au core (diameter ∼2 nm), a passivating Au−S interface, and functionalized alkanethiol chains. Cationic and anionic AuNPs have been modeled with amine and carboxyl terminal groups and Cl^-/Na^+ counterions, respectively. The radial distribution functions show that the side chains and terminal groups show significant flexibility. The orientation of water is distinct in the first solvation shell, and AuNPs cause a long-range effect in the solvent structure. The radial electrostatic potential displays a minimum for $AuNP^-$ at 1.9 nm from the center of the nanoparticle, marking a preferable location for Na^+, while the $AuNP^+$ potential (affecting the distribution of Cl^-) rises almost monotonically with a local maximum. Comparison to Debye−Hückel theory shows very good agreement for radial ion distribution, as expected, with a Debye screening length of about 0.2−0.3 nm. Considerations of zeta potential predict that both anionic and cationic AuNPs avoid coagulation. The results highlight the importance of long-range electrostatic interactions in determining nanoparticle properties in aqueous solutions. They suggest that electrostatics is one of the central factors in complexation of AuNPs with other nanomaterials and biological systems, and that effects of electrostatics as water-mediated interactions are relatively long-ranged, which likely plays a role in, e.g., the interplay between nanoparticles and lipid membranes that surround cells.

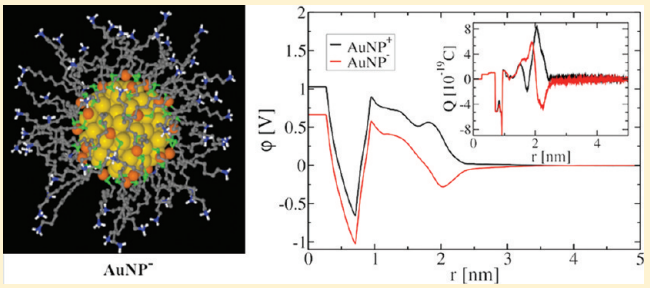

INTRODUCTION

Nanoparticles (NPs, size range 1−100 nm) have many interesting properties, as they bridge the gap between bulk materials and atomic or molecular structures.[1,2] Typically, the physical properties of bulk materials do not depend on the size of the sample, while at the nanoscale size-dependent properties are frequently encountered. Two contributing factors for the size dependence are (a) number of surface atoms whose percentage reduces as the NP size increases toward the bulk limit and (b) quantum confinement effects at the smallest length scales (<10 nm) where the electronic structure plays a significant role in determining the composition, stability, structure, and function of NPs.[3,4]

Nanoparticles often display fascinating optical properties because of quantum effects, and, e.g., gold nanoparticles (AuNPs) appear from yellow to deep red and black in solution depending on their size.[5] In photovoltaic cells, absorption of solar radiation is much higher for semiconductor materials comprised of NPs than for continuous sheets of thin films (e.g., CdTe, ZnO).[6] For phase-change materials used in optical data storage and nonvolatile computer memory, chalcogenide (e.g., GeTe) NPs offer an intriguing route of manufacturing composite materials with tuned (size-dependent) melting point and recrystallization temperature.[7] Other size-dependent properties include surface plasmon resonance in metal NPs,[8] quantum confinement effects in semiconductor NPs (quantum dots),[9] and superparamagnetism in magnetic materials.[10] The changes in physical properties are not always desirable, and,

Received: February 2, 2012
Revised: April 6, 2012

   dx.doi.org/10.1021/jp301094m | J. Phys. Chem. C XXXX, XXX, XXX−XXX

e.g., the magnetization direction of small ferromagnetic NPs can switch at low temperature, making them unsuitable for applications.[11]

Several nanoparticles are used in nanomedicine and biochemistry for drug delivery, diagnostics, therapeutics, and bioimaging.[12−17] AuNPs are one type of nanoagents that are being employed for such purposes,[18−22] and they have nowadays a variety of useful applications in these fields. Meanwhile, according to recent experimental findings, AuNPs may also have cytotoxic properties (among other particle types).[23,24] In this context, the interaction between NPs and cell membranes is very relevant,[18,25−31] since all trafficking between the cell interior and the extracellular space takes place through the cell membrane.[32] The permeation rates of particles translocating through a membrane are therefore affected by the membrane potential, which in mammalian cells is known to be rather complicated and arises from asymmetric lipid[33−35] and ion distributions[34−38] on the extracellular and cytosolic sides of a cell.

Interactions of charged or polar NPs with the cell membrane are expected to be strong and long-ranged. This view is quite relevant, since NPs are often layered (protected, passivated) for medical applications, and, e.g., grafting polar surface groups onto AuNPs affects their water solubility and ability to penetrate cell membranes.[23] Extracellular positively charged NPs (e.g., SiO_2, TiO_2, AuNPs) have also been reported to intrude through cell membranes, and, in some cases, to cause a large-scale cell death in comparison with the negatively charged particles which remain on the extracellular side.[12,13,19,20,23,24] It has been concluded that, among other factors, such as NP size/shape and hydrophobicity of grafted side chains, toxicity of nanoparticles depends on the sign of charge.[24,39] Also important to stress is the interaction of NPs with native biological molecules in the context of natural organic matter (NOM), since, e.g., carbon nanoparticles have been found to induce cell death when cells have been exposed to fullerenes together with NOM.[40]

A particularly suitable strategy to gain a better understanding of NP properties in aqueous and biological environments is to employ atomic-scale computer simulations to characterize the properties of the commonly used nanomaterials. In this spirit, not only the novelty of the topic but also the importance of revealing the details of interactions at the cellular level makes studies of *monolayer-protected AuNPs* interesting. Recently, a few molecular dynamics (MD) simulations have been performed for related systems: The properties of monolayer-protected AuNPs in water have been studied by 1 ns MD simulations,[29] and the interface between AuNP and polymers has been simulated in order to achieve all-atom models for AuNP−polymer nanocomposites (polymeric memory devices).[41] AuNP penetration in lipid bilayers has been simulated with coarse-grained (CG) MD by enforcing AuNP intrusion via external potentials, and considerable disruptions of cell membranes have been reported, including a large hole of ∼5.5 nm diameter with a positively charged AuNP.[28,31] Furthermore, while the knowledge of the effects of AuNPs on lipid membranes is rather limited, quite a lot of potentially useful insight is available from recent MD simulations of lipid membranes interacting with carbon NPs.[42]

In this work, we have performed a series of MD simulations for monolayer-protected AuNPs in aqueous solution with functionalized (charged) alkanethiol side groups [$Au_{144}(SR)_{60}$, where R = $C_{11}H_{22}$ + amine/carboxylate terminal group] to study their structural and dynamical properties, and the interaction with solvent (water, counterions). Both the cationic and anionic AuNPs were simulated over an extensive period of 200 ns, allowing us to compare the two cases on equal footing and without considerable concerns of sufficient sampling. The nanoparticle composition corresponds to one of the most ubiquitous synthesized AuNP sizes (29 kDa, core diameter ∼2 nm), matching also its mass-spectrometrical analysis for $Au_{144}(SR)_{60}$.[43−46] Also, the AuNP structure incorporates the common structural details reported for several cluster sizes in this size regime ($d \leq 2$ nm).[3,47−50] The structural model of $Au_{144}(SR)_{60}$ is based on the recent theoretical model by Lopez-Acevedo et al.[51] which was shown to be in very good agreement with the experimental X-ray powder diffraction measurements,[52] and the AuNP electronic structure is consistent with the chemical voltammetry measurements and optical properties.[43,53,54]

We discuss several aspects of electrostatics in systems comprised of charged nanoparticles and ions in aqueous environments. We consider the ordering and dynamics of ions and water around AuNPs, and the range of water-mediated interactions between AuNPs and other objects. We also discuss ions' distributions in terms of the Debye−Hückel description and use this treatment for consideration of nanoparticle coagulation in terms of the zeta potential. Overall, our results emphasize the importance of electrostatics and the interface between AuNP and solvent as decisive factors in determining the properties of nanoparticle complexes in aqueous environments. In this spirit, the present work provides a basis for further investigations of the $Au_{144}(SR)_{60}$ nanoparticles in biologically relevant interface systems such as lipid membranes.

MATERIALS AND METHODS

Descriptions of Model Systems. Monolayer-protected gold nanoparticles (AuNPs) of 144 Au atoms have been modeled with functionalized alkanethiol side groups (undecanyl chain, R = $C_{11}H_{22}$, and a terminal group), shown in Figure 1. The alkanethiol chains are modeled on the basis of the united atom concept that describes a CH_2 group as a single "united" bead. The rigid 114-atom gold core possesses a nearly-spherical polyhedral geometry (rhombicosidodecahedron) based on the previous theoretical suggestion.[51] The monolayer covering the Au core consists of 30 "oxidized" surface gold atoms and 60 alkylthiol ligands (SR−, with R = $C_{11}H_{22}$) with polar terminal groups, and two ligands attached to each surface gold atom (Figure 2). (As a remark, let us mention that rigorously speaking there is no "alkyl" chain here in a traditional sense due to the S atom in the given functional group, but we use this naming convention here.) This feature of the Au−S interface, which exists also for self-assembled monolayers on bulk Au, has not been incorporated previously for AuNP simulations with classical force fields.[28,29,31,41] Two types of Au nanoparticles were prepared: one with a terminal amine group (NH_3^+) and the other with a carboxylic group (COO^-) attached to each hydrocarbon chain (Figure 1). The molecular formulas of the corresponding particles can be represented as $Au_{144}(SRNH_3^+)_{60}$ and $Au_{144}(SRCOO^-)_{60}$ for $AuNP^+$ and $AuNP^-$, respectively.

The simulation box dimensions were adjusted for all systems to 7.06 × 7.06 × 7.06 nm^3. After placing the AuNP inside the box, the box was filled with water, and 60 counterions were added for each AuNP: Cl^- ions for $AuNP^+$ and Na^+ ions for $AuNP^-$. The chosen system size was confirmed to be consistent

dx.doi.org/10.1021/jp301094m | J. Phys. Chem. C XXXX, XXX, XXX−XXX

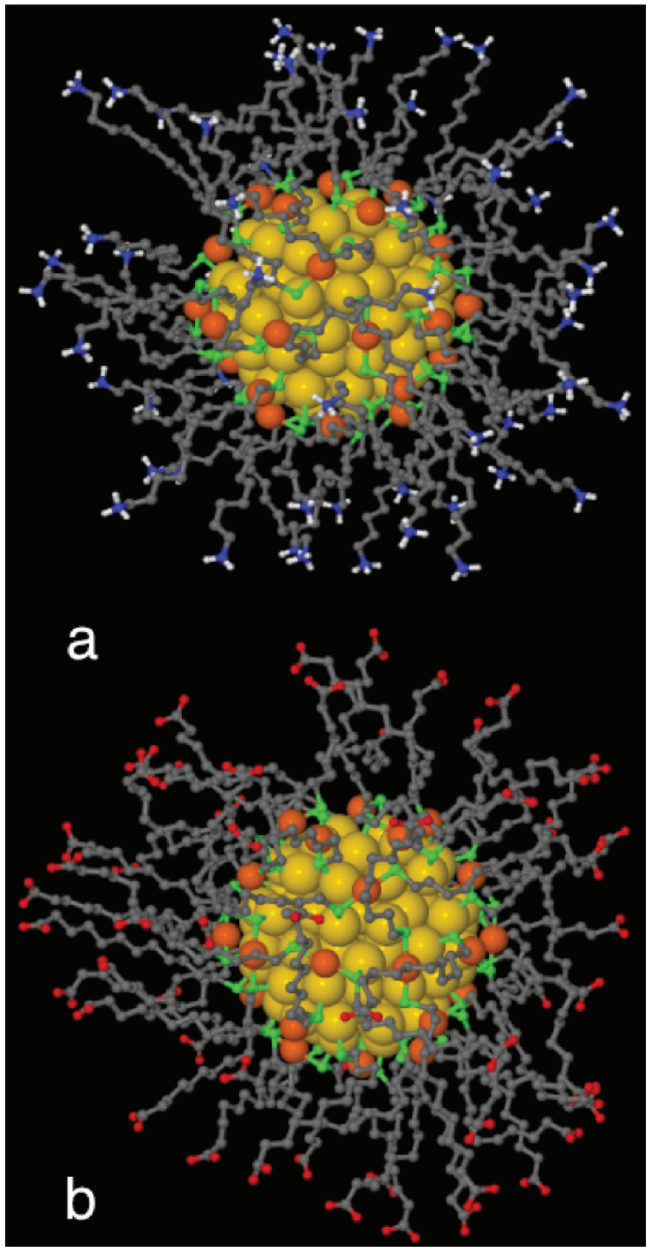

Figure 1. Visualization of Au nanoparticles: (a) the cationic $Au_{144}(SRNH_3^+)_{60}$ and (b) the anionic $Au_{144}(SRCOO^-)_{60}$, where R = $C_{11}H_{22}$. Color code: Au (core), gold; Au (interface), orange; S, green; C (united atom), gray; N, blue; O, red; and H, white.

with the water density at the given temperature. The overall number of atoms in the simulated systems was around 33 000.

Our long-term goal is to model interactions of functionalized AuNPs with cell (lipid) membranes, and the AuNP force-field has to be consistent with the force-field for lipid membranes. As follow-up simulations of AuNPs with lipid membranes are currently in progress, we here describe the background related to both simulation projects. We employ the well-known united-atom force-field by Berger et al.[55] for the alkythiol side groups. The force-field is essentially a mixture of OPLS (nonbonded interactions) and GROMOS (bonded interactions) force-fields. Partial charges for the ionized head groups of $AuNP^+$ and $AuNP^-$ were taken from the appropriate parts of POPE[55,56] and POPS[57] lipids, respectively. A common problem for metallic NPs in a biologically relevant environment is the fact

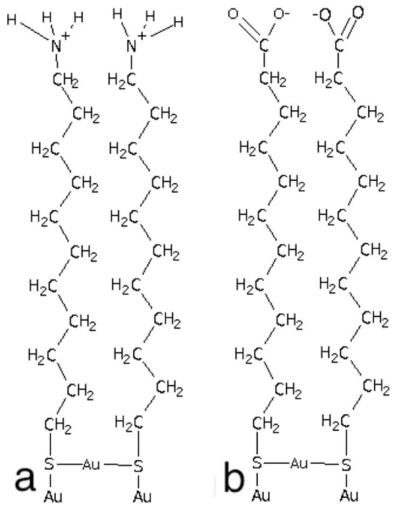

Figure 2. Schematic description of the atom nomenclature of alkanethiol groups: (a) $AuNP^+$ with amine and (b) $AuNP^-$ with carboxylic terminal group (charged). Pairs of hydrocarbon chains are connected via one Au (surface) in each case, and the RS−Au−SR oligomers (R standing for the hydrocarbon chain) make additional Au−S bonds with the Au core. CH_2 groups are treated using the united-atom description.

that metals are not normally included in biomolecular force-fields. Recently, Lennard-Jones (LJ) parameters for several metals were developed,[58] and the parameters are compatible with some widely used empirical force-fields, such as Charmm, Amber, and OPLS. Therefore, the corresponding OPLS-compatible LJ parameters for Au atoms were taken from ref 58. Partial charges of the AuNP core (144 Au and 60 S atoms) were evaluated from the density functional (DF) calculations of ref 51 by using electron density and the method of Bader charges. The rigidity of the gold core was preserved by introducing a number of virtual constant bonds and constraint potentials between Au atoms of the core. Additional bonds and constraint potentials were set for the Au−S interface structure in order to maintain the correct geometry of the NP interior (details given in the Supporting Information).

Water molecules were represented using the SPC model.[59] The particle-mesh Ewald summation (PME) method[60] was used for the electrostatic interactions with a real space cutoff of 1.0 nm and a reciprocal grid of 60 × 60 × 60 cells with a fourth-order *B*-spline interpolation. For van der Waals interactions, we used a cutoff distance of 1.0 nm. All MD simulations were performed by using the GROMACS package (version 4.0.5).[61]

Prior to actual simulations, the systems were energy minimized and equilibrated by short 20 ns MD runs. The production simulations were performed over a period of 200 ns for each AuNP. For comparison, previous simulation studies of related systems covered time scales of the order of 1 ns.[29] The time step was set to 1 fs, and the neighbor list (cutoff 1.0 nm) was updated for every frame. The simulations were performed both in the *NVT* and *NPT* ensembles for 200 ns, respectively. For the *NVT* ensemble, the temperature was set to 310 K using the Berendsen thermostat[62] with a time constant of 0.1 ps. In addition, for the *NPT* ensemble, the Berendsen algorithm[62] with a compressibility of 4.5×10^{-5} bar^{-1}, time constant of 5 ps, and reference pressure of 1 bar was used for isotropic pressure coupling. The variable cell size in *NPT* resulted in 0.02−0.03 nm changes in the simulation box dimensions (7.06 nm). However, most of the analysis was performed using the

dx.doi.org/10.1021/jp301094m | *J. Phys. Chem. C* XXXX, XXX, XXX−XXX

NVT simulation data (constant simulation box size) for practical reasons, mainly due to determination of the electrostatic potential (see below) where a constant system size is most appropriate. In practice, several tests showed that the difference between the *NVT* and *NPT* simulation data was negligibly small. Self-diffusion coefficient values shown in this article are calculated using *NPT*, since the movement of the molecules and particles is considered to be more realistic under constant pressure. The diffusion coefficients of the *NVT* ensemble are shown in Table 1 in the Supporting Information.

Analysis. Data for analysis was stored every 10 ps (RDF, ESP, diffusion coefficients, water orientation). Furthermore, in order to study particularly rapid processes related to hydrogen bonds (water) and other contacts (counterions) between the AuNPs and the surrounding solution, a set of five 1 ns MD simulations starting at 80 ns were performed storing data every 0.5 ps. The GROMACS suite of programs was used for the data analysis,[61,63] complemented by analysis codes of our own.

The NP size was calculated as a time average of the average distance per time frame between the center of mass of the Au core and the terminal groups. The terminal group atoms for the cationic and anionic NP are the amine hydrogens and the carboxylic oxygens, respectively. The Au core size was calculated in a similar manner as an average distance between the center of mass of the core and the surface Au atoms.

The electrostatic potential (ESP) of the systems was calculated in two ways to ensure the consistency of results. The first method takes advantage of the spherically symmetric topology of the system. In this case, the radial electrostatic potential (φ) is calculated as follows:

$$\varphi(r) = \int_0^r \mathbf{E}(r')\, \mathrm{d}r' \tag{1}$$

where $\mathbf{E}(r)$ can be calculated as follows using the Gauss theorem:

$$\mathbf{E}(r) = \frac{Q_r}{4\pi\varepsilon_0 r^2} \tag{2}$$

Here, Q_r is the total charge enclosed by a sphere of radius r from the AuNP center and ε_0 stands for the dielectric constant. The used grid size has been 0.001 nm to calculate Q_r. No significant changes were observed when decreasing the grid size further.

The second method consists of the direct solution of the Poisson equation by using discrete Fourier transforms. Here, AuNP is centered in a three-dimensional grid where the atomic charges are placed by linear interpolation. The charge density grid is Fourier transformed afterward. By applying eq 2 and inverse-Fourier-transforming the potential in the reciprocal space (with wave vectors $\mathbf{k}_x$, $\mathbf{k}_y$, $\mathbf{k}_z$), one obtains the three-dimensional electrostatic potential of the system:

$$\hat{\varphi}(\mathbf{k}_x, \mathbf{k}_y, \mathbf{k}_z) = \frac{\hat{\rho}(x, y, z)}{\varepsilon_0(-k_x^2 - k_y^2 - k_z^2)} \tag{3}$$

where $\hat{\rho}$ stands for the charge density, and in the computation one has used an equally spaced grid of 100 nodes in each direction (grid spacing being 0.07 nm). This method is significantly less sensitive to the grid size than the double integration above, and grids of 50 (0.14 nm) or 200 nodes (0.035 nm) were found to provide essentially the same results. As for the two methodologies for ESP calculation, in both cases, averages over all MD frames were performed. Importantly, the two approaches to compute ESP provided consistent results in every case. The data presented in this paper is based on the first (radial integration) technique presented in eqs 1 and 2.

Radial distribution functions (RDFs) were calculated as a function of the radial distance from the center of mass (COM) of the Au core, r. The radius of gyration, $R_g(t)$, and the moment of inertia (MOI) vector autocorrelation function (ACF), $C(t)$, were computed for the AuNP's x, y and z axes as a function of time, and for explicitly mass weighted atoms (Figure 1, Supporting Information). Similarly, the rotational correlation function (Figure 2, Supporting Information) was evaluated as a function of time, and it shows a decaying trend during the 200 ns simulation.

The analysis of hydrogen bonds (H-bonds) and ionic contacts of the AuNP terminal groups and solution was carried out by averaging over five time windows using five snapshots of the total trajectory as starting structures for 1 ns simulations with a data storage rate of 1/(0.5) ps. Contacts between the AuNP terminal groups and water molecules were considered within a cutoff distance of 0.35 nm for non-hydrogen atoms and a H-bond angle of 30°. Ion contact analysis of the AuNP solutions was performed considering ions within a cutoff distance of 0.35 nm from AuNP terminal groups.

To determine the lifetimes of hydrogen bonds, we used the approach suggested by van der Spoel et al.[63] In essence, the lifetime of a hydrogen bond τ_{HB} was given by inverse forward rate constant k through $\tau_{HB} = 1/k$. The parameter k was determined as follows. The hydrogen bonds during the simulations were allowed to break and reform, allowing us to analyze lifetimes by using binary function $h(t)$, which is 1 when a hydrogen bond is present and 0 otherwise. Then, the forward rate constant k for hydrogen bond breakage and the backward rate constant k' for hydrogen bond formation were determined from the reactive flux correlation $K(t) = kc(t) - k'n(t)$, where $c(t)$ is the autocorrelation function of $h(t)$ and $n(t)$ is the probability that a hydrogen bond that existed at $t = 0$ is broken, but the groups forming the hydrogen bond are still within the hydrogen bonding distance. For details of the lifetime determination, see ref 63.

Self-diffusion coefficients D_A of particles A were calculated by using the Einstein relation.[64] One first defines the mean-squared displacement $\mathrm{MSD}_A(t)$ as follows:

$$\mathrm{MSD}_A(t) = \langle |\mathbf{r}_i(t) - \mathbf{r}_i(0)|^2 \rangle_{i \in A} \tag{4}$$

and then the diffusion coefficient is given by

$$D_A = \lim_{t \to \infty} \frac{\mathrm{MSD}_A(t)}{6t} \tag{5}$$

where in practice we have carried out a linear fitting of the mean-squared displacement between a time interval of 20−180 ns. The error estimate is the difference of the diffusion coefficients obtained from fits over two halves of the initial fitting interval.

To characterize the diffusive motion of water and ions around AuNP, we computed their short-time diffusion factor M radially inside AuNP-centered spherical shells of thickness Δr = 0.5 nm. That is, at every time t during the simulation, we determined the water molecules and ions that at this moment t were at a given distance from the center of AuNP, after which we determined their mean-squared displacement over a short period of time; the width of the time window was Δt = 200 ps and Δt = 500 ps for water and counterions, respectively. The

dx.doi.org/10.1021/jp301094m | J. Phys. Chem. C XXXX, XXX, XXX−XXX

data for MSD(t) in every shell (representing a fixed distance from the AuNP center) was averaged separately for water molecules and ions over the total simulation time of 200 ns. Finally, we computed the short-time diffusion factor M as an effective slope of the mean-squared displacement over the short time window. Hence, the factor M is computed largely in a similar manner as the hydrodynamic diffusion coefficient in eq 5 but now without the long-time limit. For the same reason, since M is not defined in the hydrodynamic long-time limit, we call it a diffusion factor instead of a true diffusion coefficient.

The orientation of water molecules was calculated for a time window of 0−200 ns for AuNP-centered spherical shells of thickness Δr = 0.2 nm using the angle α between a vector from the AuNP center to a water oxygen and a vector from the oxygen to a midpoint between two water hydrogens in the same molecule.

RESULTS

Structural details around AuNPs can be extracted from analyzing the three-dimensional radial distribution functions (RDFs) shown in Figure 3. Each panel depicts the RDFs with

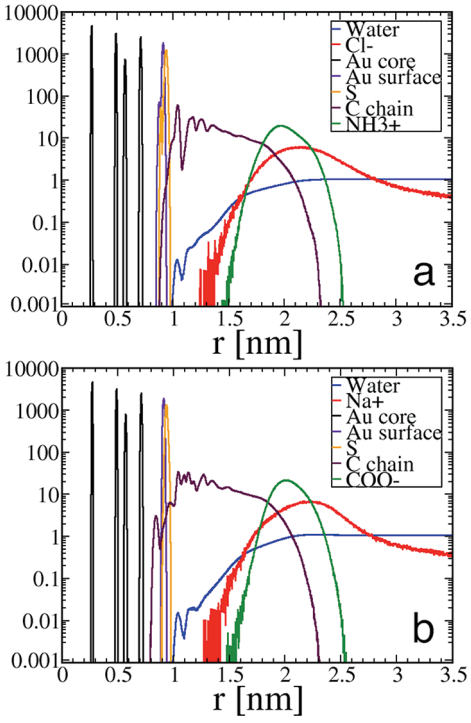

Figure 3. Radial distribution functions (RDFs) averaged over a time window of 200 ns: (a) AuNP$^+$ and (b) AuNP$^-$ solutions. The distance of r = 0 corresponds to the center of the nanoparticle.

respect to the AuNP center for relevant groups in the AuNP$^+$ (Figure 3a) and AuNP$^-$ (Figure 3b) solutions. The size (diameter) of the Au-rich part is d = 1.82 nm, and the average overall diameter is 4.06 and 4.13 nm for AuNP$^+$ and AuNP$^-$, respectively, including the alkanethiol chains and terminal groups.

The three stacked polyhedral Au layers that constitute the metallic core (114 atoms, rhombicosidodecahedron) can be clearly identified. The first two shells of the core consist of 12 and 42 atoms, respectively. One should note that the first peak corresponds to the first Au layer, while the second and third peaks reflect the second Au layer (MacKay icosahedron). The fourth peak at 0.7 nm corresponds to the outer layer of the Au core and gives an estimate for the metallic core. Between 0.9 and 1.0 nm, we find S and Au (surface) atoms according to their colinear positioning in the RS−Au−SR oligomers (Figure 2), as suggested by electronic structure calculations and X-ray diffraction measurements for AuNPs.[3] In our model, additional constraints (together with added nonbonded parameters) maintain the correct surface structure of the Au core, Au surface atoms, and S atoms (see the Supporting Information). Otherwise, these atoms would overlap because of lacking repulsive forces.

The average hydrocarbon chain length is 1.16 and 1.17 nm for AuNP$^+$ and AuNP$^-$, respectively, measured as the distance between the first carbon (connected to S) and the amine nitrogen or carboxylic carbon, respectively. Correspondingly, for a single unit of the alkyl chain, CH_2, the segment length is 0.096 nm for both AuNPs. The radius of gyration is R_g = 0.946 ± 0.004 nm and R_g = 0.995 ± 0.005 nm for AuNP$^+$ and AuNP$^-$, respectively. These values are biased toward the Au core because of the large atomic mass of gold.

ESP and the radially integrated charge of the AuNP solutions are presented in Figures 4 and 5 (see also Figures 6 and 7 in the

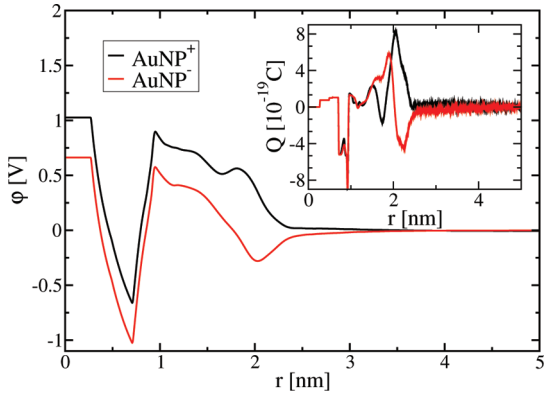

Figure 4. Radially integrated electrostatic potential and charge (the latter shown in the inset) in AuNP solutions.

Supporting Information). Both particles comprise the same Au_{114} core and Au−S interface, and they essentially display the same distribution of accumulated charge in the core region (<1 nm, Figure 4, inset). Small differences can be detected due to the mobility of the interfacial Au and S atoms. Between 1.0 and 1.3 nm, a small flat region is observed accounting to the neutral carbons (united atoms, Figure 2) of the alkyl chain. After this, the COO^- and NH_3^+ terminal groups start to contribute, and the graphs substantially differ. These differences can be understood by comparing the individual RDFs of the terminal groups and their respective partial charges (Figures 2 and 3).

ESP analysis shows that in the AuNP$^-$ system the counterions (Na^+) are likely to accumulate around 2.0 nm from the AuNP center, where an ESP minimum is observed. For AuNP$^+$, the counterions (Cl^-) experience an almost monotonically increasing (attractive) ESP toward the center with a small maximum. Here, one should remember to invert the curve when testing the effects for negative counterions. Obviously, ESP accounts only for the electrostatic forces and neglects details at the atomic level. The RDFs of the counterions in Figure 3 show that both curves mainly overlap instead of finding Cl^- significantly closer to the AuNP core, as

dx.doi.org/10.1021/jp301094m | J. Phys. Chem. C XXXX, XXX, XXX−XXX

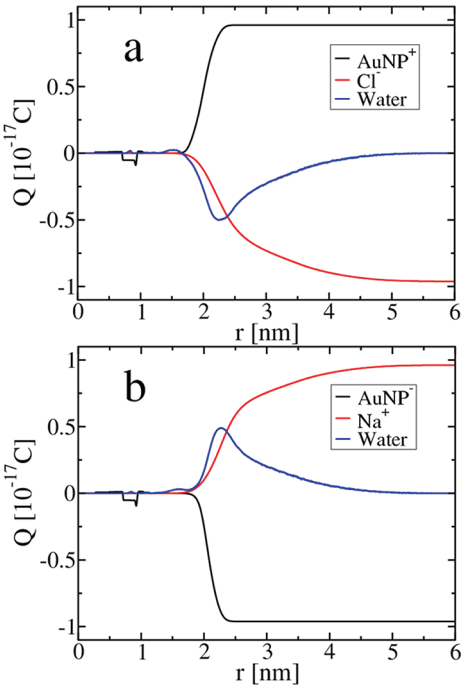

Figure 5. Radially integrated charge in AuNP solutions decomposed into the different components.

one would expect based on ESP. The underlying reason is that, despite the stronger attractive electrostatic force toward the core, Cl^- is also substantially larger than Na^+ in size (cf. the atomic radii, 0.098 nm in Na^+ and 0.181 nm in Cl^-). As a consequence, Cl^- experiences a stronger repulsion when trying to penetrate inside the hydrocarbon chain region. The ion size effect and ESP balance each other, leading to rather similar RDF behavior for both AuNPs.

When the radially integrated charge is decomposed into different components due to the AuNP, water, and ions, one finds (see Figure 5) the contribution due to the nanoparticle to compete against the other two factors. The contribution of ions decays slowly as expected on the basis of the above RDF data. More interesting is the behavior of water, since it shows a peak with a width of about 2 nm, the peak position being close to the maximum of ion distribution (see Figure 3). As further results below for the distribution of water orientation will show, the water behavior in Figure 5 largely arises from the complexity of the ordering of water. Similar features over similar scales have been observed for water close to its interface with charged lipid membranes.[65]

One of the exciting topics in electrolyte solutions concerns the distribution of ions around other charged objects.[66] In the present case with counterions, the proper theoretical context is given by the (mean-field) Debye–Hückel (DH) theory, where for counterions around a charged particle, one combines the Poisson equation to specify the electrostatic potential of an ion with the Boltzmann equation for charge distribution. In radial symmetry, the Debye–Hückel description for the counterion distribution around a charged NP reads as $Ae^{-Br}/r + C$, where A, B, and C are (positive) constants. Here, the constant C is included due to finite system size. However, the most relevant parameter for our purposes is $1/B = \kappa$, known as the Debye screening length.

As our data for counterion distributions were fitted to the DH description, the agreement was found to be very good at large distances (see Figure 6), as expected. Here, it is important to briefly comment on the statistics of the distributions, since

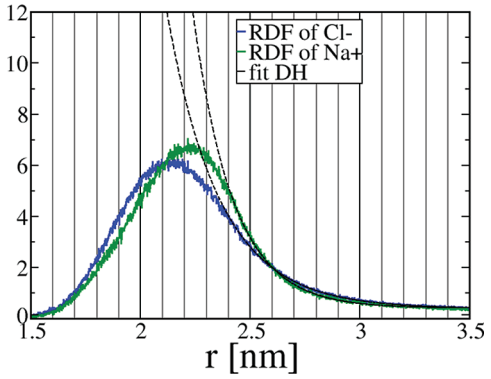

Figure 6. Counterion distribution profiles fitted to the Debye–Hückel description. The RDFs of counterions Cl^- and Na^+ are drawn using blue and green color, respectively. The exponential fits based on the Debye–Hückel theory, $Ae^{-Br}/r + C$ with constants A, B, and C are drawn using black dashed lines. The fits were made for data with $r \geq 2.5$ nm.

the number of ions was limited to 60 to neutralize the functional groups of the AuNP.

The number of ions is not a problem, since the data given below for ion-AuNP lifetimes (Table 1) show that the contacts

Table 1. Hydrogen Bonds and Ionic Contacts between AuNP and Solvent[a]

A	N_A	τ_A (ps)
water ($AuNP^+$)	170.8 ± 0.2	6.5 ± 0.2
Cl^-	4.7 ± 0.4	5.0 ± 0.1
water ($AuNP^-$)	404.4 ± 0.5	3.5 ± 0.1
Na^+	4.4 ± 0.4	10.1 ± 1.1

[a] N_A is the average number of hydrogen bonds and contacts, and τ_A is the average lifetime of the contacts.

between ions and the AuNP are rapid, and the diffusion of ions is also fast (Table 2), indicating that the statistics during the 200 ns simulations for the ion distributions are quite substantial.

Table 2. Self-Diffusion Coefficients D_A of Particles A in AuNP Solutions in the *NPT* Ensemble

A	D_A[× 10^{-5} cm^2 s^{-1}]
$Au_{144}(SRNH_3^+)_{60}$	0.2 ± 0.1
water	4.7 ± 0.1
Cl^-	1.6 ± 0.2
$Au_{144}(SRCOO^-)_{60}$	0.1 ± 0.1
water	4.7 ± 0.1
Na^+	1.0 ± 0.1

The deviations between the ion distribution data and the DH descriptions emerge around 2.4 nm from the AuNP center of mass, which can be considered as an approximate location for the interface (often called a double layer) between NP-bound and loosely associated counterions, the latter being able to move rather freely in the system despite the presence of the NP. The fits shown in Figure 6 yield values of 0.27 and 0.20 nm

dx.doi.org/10.1021/jp301094m | J. Phys. Chem. C XXXX, XXX, XXX–XXX

for the Debye length in $AuNP^+$ and $AuNP^-$, respectively. These lengths are 1 order of magnitude smaller than the NP size, which implies that the assumptions of the Smoluchowski theory for zeta potential determination are valid in the present case.

Now, assuming 2.4 nm to be a safe (that is likely too large) estimate for the position of the interface between NP-bound and loosely bound ions, the ESP gives an approximate estimate for the zeta potential: 26 mV for $AuNP^+$ and −59 mV for $AuNP^-$ (see Figure 8, Supporting Information). The different numbers highlight that cationic and anionic AuNPs respond to an external field with different strengths. Further, even if our assumption of the location of the interface were partly inaccurate, we can still conclude that the zeta potential in the present systems without salt is about 25 mV, or larger than this value, which is often considered as a threshold value for coagulation/aggregation. Further, if there were salt, the Debye length would decrease for increasing ion concentration, which would show up as an increase in the zeta potential (see Figure 8, Supporting Information). Recent experimental data by Verma et al. for gold nanoparticles protected by a number of different organic ligands is in agreement with this view, since they found[23] the (absolute value of) zeta potential to vary between ∼31 and 38 mV. Summarizing, our analysis predicts that the AuNPs considered in this work do not coagulate.

The AuNP terminal group contacts with water and counterions are visualized in Figures 7 and 8. The average number of H-bonds and ion contacts per 0.5 ps time frame and their lifetimes are shown in Table 1. The analysis of H-bonds and ion contacts with the terminal groups reveals differences between the two AuNP systems. The terminal amine groups of $AuNP^+$ form three contacts with the solvent each. There are two possible configurations: First, one hydrogen of NH_3^+ connects to a counterion Cl^- and the other two form H-bonds with water oxygens (Figure 7b), and second, the amine hydrogens make three H-bonds with water oxygens (Figure 7c). The solvent configurations around the terminal carboxyl groups of $AuNP^-$ appear more complicated, as they form six or seven contacts (Figure 8). One frequent case is a configuration of seven H-bonds between the carboxyl group and seven waters. Another relevant configuration involves contacts between Na^+, COO^-, and water in such a way that the two carboxylic oxygens form H-bonds with four waters and two (ionic) Na−O bonds with the counterion, and in addition, Na^+ forms four ionic Na−O bonds with the nearby waters (Figure 8b,c).

The average number and the lifetime of H-bonds and ion contacts (Table 1) show a significant difference between the two AuNP solutions: The total number of H-bonds between water and AuNP is 170.8 ± 0.2 and 404.4 ± 0.5 for the cationic and anionic AuNP, respectively, and the number of contacts for the anionic case is over 2 times larger. Nevertheless, the total number of ion contacts does not differ considerably (4.7 ± 0.4 and 4.4 ± 0.4 for $AuNP^+$ and $AuNP^-$, respectively). These results are consistent with the details of the atomic configurations around the terminal groups (discussion above); the number of contacts with water is over 2 times larger for the COO^- groups ($AuNP^-$) because each carboxyl oxygen is able to make several H-bonds simultaneously. The number of counterions around terminal groups is similar (the total number of opposite charges inside the simulation box is the same, 60), but when it comes to contact lifetimes, the results reveal differences in counterion coordination. The AuNP/counterion contact lifetime is 5.0 ± 0.1 and 10.1 ± 1.1 ps for the cationic and anionic AuNP, respectively. The Na^+ ions (with $AuNP^-$) are more tightly bound, between two COO^- oxygens and surrounded by water molecules (Figure 8), whereas the Cl^- ions ($AuNP^+$) are more mobile, as they are bound to only one NH_3^+ hydrogen (Figure 7). The water contact lifetimes are longer for the cationic nanoparticle, 6.5 ± 0.2 vs 3.5 ± 0.1 ps, and this appears to be coupled to the ion coordination. The water contacts of $AuNP^+$ are less disturbed by counterion movements (weaker ion binding of the NH_3^+ group and fewer H-bonds), and hence, the lifetime value of water is larger.

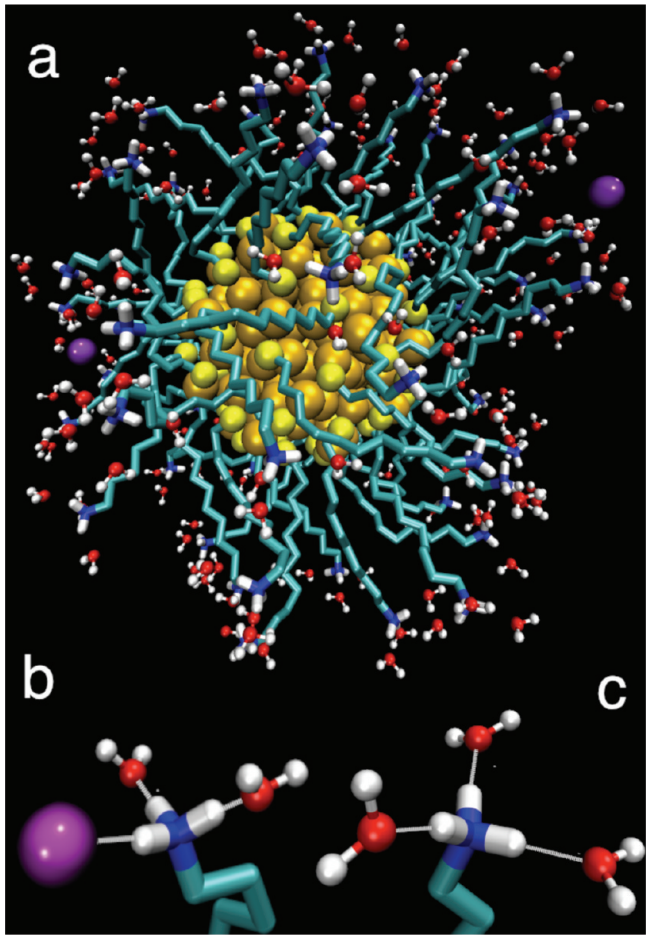

Figure 7. The first solvation shell of $AuNP^+$: Amine terminal groups NH_3^+ with Cl^- counterions and water. (a) The cationic AuNP and solvent molecules within a cutoff distance of 0.34 nm. (b) NH_3^+ terminal group (color key: N, blue; H, white) forming three contacts: one ionic bond with Cl^- (violet) and two H-bonds with water molecules (O, red). (c) NH_3^+ group forming H-bonds with three water molecules.

The self-diffusion coefficients of the AuNP solution in the *NPT* ensemble are presented inTable 2 (see also Table 1 in the Supporting Information for the diffusion coefficients in the *NVT* ensemble), and the corresponding MSD curves are shown in Figure 9 in the Supporting Information. The diffusion coefficients show no significant difference for water. The water molecules were represented using the SPC model in the simulation setup, and the previously reported diffusion coefficient for (pure) SPC water 4.40 × 10^{-5} cm^2 s^{-1} is smaller than that for the AuNP solutions,[67] but so is also the temperature 300 K compared to the one in our work (310 K). The minor difference therefore arises in part from thermal

dx.doi.org/10.1021/jp301094m | J. Phys. Chem. C XXXX, XXX, XXX−XXX

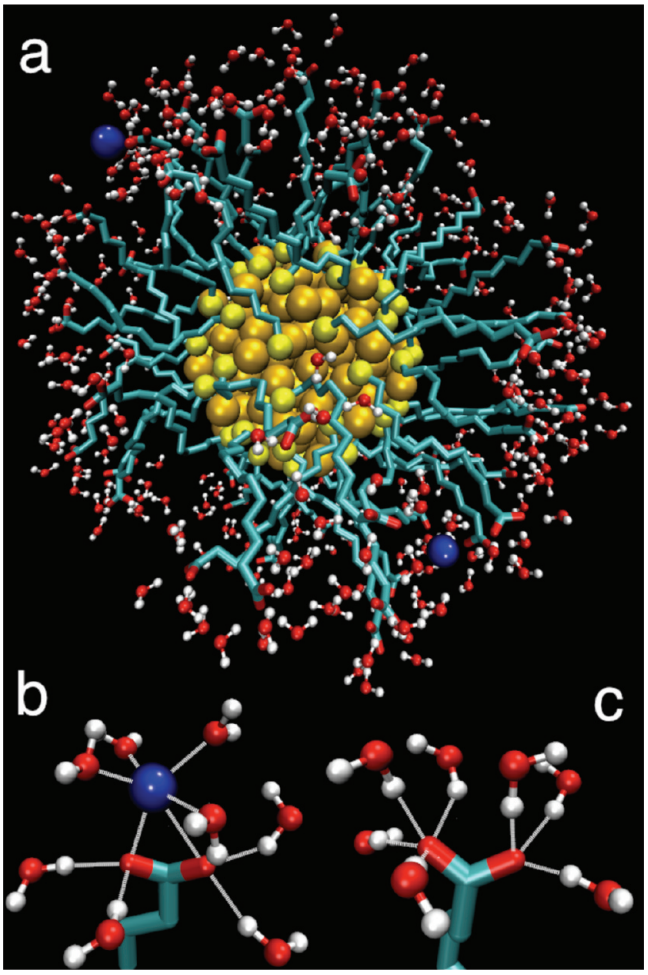

Figure 8. The first solvation shell of $AuNP^-$: Carboxylic terminal groups COO^- with Na^+ counterions and water. (a) The anionic AuNP and solvent molecules within a cutoff distance of 0.36 nm. (b) Na^+ ion (color: blue) is coordinated by four water molecules (O, red; H, white) and COO^-, and the two carboxylic group oxygens form H-bonds with four waters. (c) COO^- group and seven water molecules; three and four H-bonds for each carboxylic oxygen.

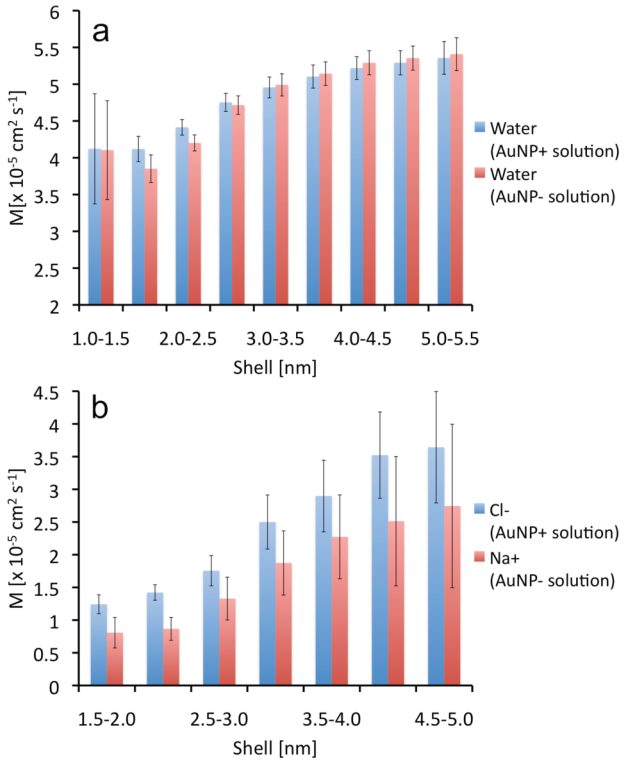

Figure 9. Solvent mobility around AuNPs in spherical shells. (a) Mobility of water and (b) counterions located at AuNP centered Δr = 0.5 nm shells for time windows of Δt = 200 ps (water) and Δt = 500 ps (counterions) averaged over the 0−200 ns simulation time. The $AuNP^+$ and $AuNP^-$ histograms are presented using blue and red colors, respectively. The error bars correspond to standard deviation.

fluctuations and the presence of AuNP and the counterions. Furthermore, the diffusion coefficient of Cl^- counterions ($AuNP^+$) is approximately 20% higher than that for Na^+ ($AuNP^-$). This shows that the counterions of $AuNP^-$ are not able to move as freely as in $AuNP^+$, which is consistent with the stronger ionic binding between the carboxylate groups ($AuNP^-$) and Na^+. This also correlates with the fact that the first hydration shell around a Na^+ ion is more ordered than that for a Cl^- ion.[68] The diffusion coefficients of $AuNP^+$ and $AuNP^-$ are almost identical given their error bars.

The short-time diffusion factors of water molecules and counterions have been determined inside spherical 0.5 nm shells around AuNPs, and they are shown in Figure 9. Apart from the slight deviation at 1.5−2.5 nm, the results show little difference for water (as for the self-diffusion coefficients, Table 2), but there is a significant deviation for the counterions. The Cl^- ions ($AuNP^+$) have higher values than those (Na^+) of the anionic nanoparticle. In general, the short-time diffusion values increase as a function of radius, which is caused by the water/ion interactions with AuNPs. The proximity of AuNP slows down the diffusion of water molecules and ions. Water forms an H-bond network around the terminal groups of AuNP (and counterions), and this makes the H_2O positions more restricted close to AuNP. For water, the rate of increase in short-time diffusion factors as a function of distance is lower than for the counterions. This can be explained by the type of bonds which water and ions form with AuNP: An H-bond between AuNP and an H_2O molecule is weaker and of shorter range than the electrostatic interaction between AuNP and a counterion.

The effect of AuNP in solvent diffusion extends at least to 5 nm from the AuNP center (3 nm from the surface, Figure 9), which indicates that the solvent transmits the interaction shell-by-shell by intermediating the orientation of water molecules. This phenomenon is evident in the solvent orientation data shown for the AuNP solutions in Figure 10. As for the short-time diffusion analysis, the water orientations also depend strongly on distance: The first shell surrounding the NH_3^+ terminal groups aligns water molecules in such a manner that oxygen is closer to $AuNP^+$ than the H atoms, and vice versa for $AuNP^-$. This effect arises from the electrostatic forces (of H-bonding) between the oppositely charged terminal groups of AuNPs and polarized water molecules, and it results in opposite trends for the two AuNPs.

■ CONCLUSIONS

Gold nanoparticles are being used extensively in biotechnology and nanosciences, and revealing the details of their interactions with biological fluids at an atomistic level is very relevant. We have performed a series of classical MD simulations for monolayer-protected AuNPs with functionalized (charged) alkanethiol side groups in aqueous solutions. It should be emphasized that the nanoparticle composition matches one of

dx.doi.org/10.1021/jp301094m | J. Phys. Chem. C XXXX, XXX, XXX−XXX

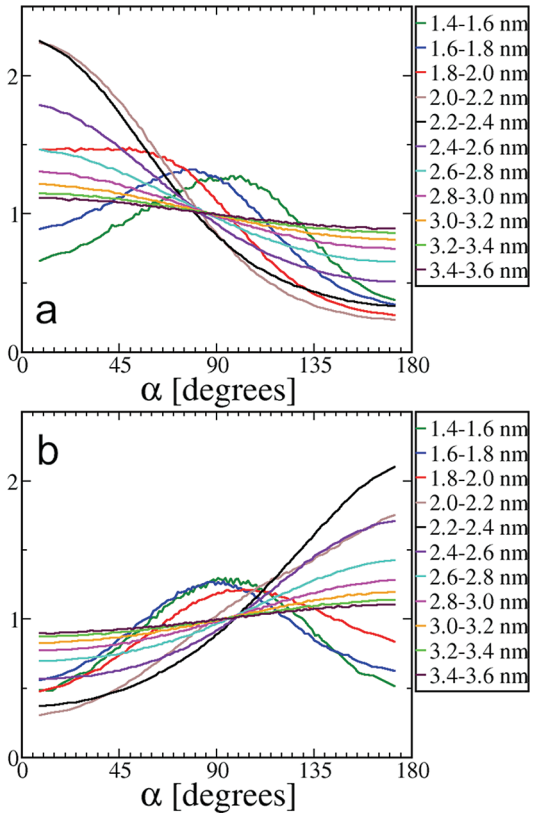

Figure 10. Distribution of water orientation for different distances from the AuNP center: (a) $AuNP^+$ and (b) $AuNP^-$. Orientation is characterized by the angle α, which is defined by a vector from the AuNP center to a water oxygen and a vector from this oxygen to a midpoint between two H atoms in the same H_2O molecule. If the two vectors are aligned pointing in the same direction, then the angle is $\alpha = 0$. Solvent orientation is calculated for AuNP centered spherical shells of thickness $\Delta r = 0.2$ nm over the simulation simulation time 0–200 ns. Note that the most likely location for the terminal groups is between 1.8 and 2.2 nm, (Figure 3).

the most ubiquitous synthesized AuNP sizes (29 kDa, ~2 nm) and its mass-spectrometrical analysis ($Au_{144}(SR)_{60}$),[43–46] and the AuNP structure incorporates the structural details observed for several cluster sizes, where the Au core is a nearly spherical polyhedron and a part of the Au atoms participate (in oxidized form) in the Au–SR ligand shell.[3]

Cationic and anionic AuNPs were modeled with amine (NH_3^+) and carboxyl (COO^-) terminal groups and Na^+/Cl^- counterions. For the two systems, RDFs (Figure 3) were found to be rather similar: The side chains and terminal groups showed significant flexibility and the water/counterion profiles had the same characteristics. However, the distance distributions of terminal groups (Figure 4, Supporting Information) showed that the NH_3^+-terminated alkyl thiols displayed a wider range of distances (fluctuations with respect to each other), and the atomic configurations (water/counterions) were significantly different around the NH_3^+ and COO^- terminal groups. The orientation of water was observed to be distinct for both AuNPs in the first solvation shell, and the AuNPs clearly caused a long-range effect in the solvent structure. This effect was particularly strong for counterions, emphasizing the importance of long-range interactions (electrostatics) in the present system.

The radial electrostatic potential profiles (Figures 4 and 5) displayed a minimum for $AuNP^-$ at about 2.0 nm from the nanoparticle center, marking a preferable location for Na^+, while the electrostatic potential of $AuNP^+$ rised almost monotonically and attracted Cl^- (in principle) further inside. However, other factors (such as reduced water concentration and larger ionic radius) exhibited Cl^- from entering inside $AuNP^+$. Despite its larger atomic mass, the self-diffusion coefficient of Cl^- was about 20% larger than that of Na^+, which is related to the details in ionic bonding with the terminal carboxylate/amine groups (reduced lifetime for Cl^- contacts). The short-time diffusion analysis around AuNPs revealed that the solvent diffusion is slower near AuNP due to H-bonds and ionic contacts with the terminal groups, and that the effect extends over 3 nm from the AuNP surface because of several solvation shells that transmit the effect.

When our data for counterion distributions were fitted to the Debye–Hückel description, we found the agreement to be very good. The interface between NP-bound and loosely associated counterions was observed to be around 2.4 nm from the AuNP center of mass, and a fit to the ion density distributions at distances larger than this one resulted in values of 0.27 and 0.20 nm for the Debye length in $AuNP^+$ and $AuNP^-$, respectively. The Debye lengths are small, and about an order of magnitude smaller than the NP size, allowing us to use the Smoluchowski theory for zeta potential determination. Consideration in this spirit results in zeta potentials of about 26 mV for $AuNP^+$ and 59 mV for $AuNP^-$. The results therefore do not support the idea of coagulation for the NPs studied here.

Concluding, our results highlight the importance of electrostatics and the nanoparticle–solvent interface in determining the properties of AuNPs considered in this work. The results provide a great deal of insight into the properties of charged and functionalized NPs in aqueous surroundings. Considering that the model used in this work is particularly realistic and is in agreement with a wide range of experiments (see the Introduction), its predictions for AuNPs are expected to be highly useful in follow-up considerations of NP effects on biological systems.

Our data show that NPs of this type cannot be considered as distinct bodies, but on the contrary, due to long-range interactions, they form complexes together with the ions and solvent molecules surrounding them. This implies that in NP solutions there are interactions between the nanoparticles due to the ordering effects of water and ions around the NPs, which give rise to long-range solvent-mediated interactions that complement those due to hydrodynamics (conservation of momentum). The significance of these effects is stressed by the fact that nanomaterials in biological environments are rarely pristine neutral particles, as instead (synthetic) NPs under these conditions are usually charged or polar. The present results may therefore have generic interest especially in biological situations where synthetic nanomaterials interact with and aim to access cells. The main barrier that they need to overcome is the cell membrane characterized by a membrane potential coupled to a cloud of salt ions. Therefore, the central issue that is worth clarifying is the interaction between NP complexes and cell membranes. On the basis of our results, the characteristic length over which charged AuNPs may affect biological molecules or complexes (such as lipid membranes) in terms of water-mediated interactions is at least ~10 nm. Depending on the NP charge and the molecular composition of the membrane, the reorganization of the lipid membrane system that results from this interplay is expected to vary. Work in this direction to clarify these issues is underway.

dx.doi.org/10.1021/jp301094m | J. Phys. Chem. C XXXX, XXX, XXX–XXX

■ ASSOCIATED CONTENT

Supporting Information

Additional data for methodology, radius of gyration, moment of inertia vector autocorrelation function, rotational correlation function, detailed radial distribution functions of AuNP terminal groups, terminal group distance distributions, mean-squared displacements of the systems, diffusion coefficients of the canonical NVT ensemble, and visualizations of the alkyl chain ends close to the Au core with overall AuNP conformations.

This material is available free of charge via the Internet at http://pubs.acs.org.

■ AUTHOR INFORMATION

Corresponding Author

*E-mail: jaakko.akola@tut.fi.

Notes

The authors declare no competing financial interest.

■ ACKNOWLEDGMENTS

We thank Pu-Chun Ke for inspiring discussions. The computations were performed on the Juropa (Intel Xeon 5570) and Cray XT4/XT5 computers in the FZ Jülich (Germany) and CSC - IT Centre for Science Ltd (Espoo, Finland). Financial support from the Academy of Finland (E.H., H.M.-S., I.V., J.A.) and the Alexander von Humboldt Foundation (A.A.G.) is gratefully acknowledged.

■ REFERENCES

(1) Daniel, M.; Astruc, D. *Chem. Rev.* **2004**, *104*, 293−346.
(2) Murray, R. W. *Chem. Rev.* **2008**, *108*, 2688−2720.
(3) Walter, M.; Akola, J.; Lopez-Acevedo, O.; Jadzinsky, P.; Calero, G.; Ackerson, C.; Whetten, R.; Grönbeck, H.; Häkkinen, H. *Proc. Natl. Acad. Sci. U.S.A.* **2008**, *105*, 9157−9162.
(4) Lopez-Acevedo, O.; Kacprzak, A. K.; Akola, J.; Häkkinen, H. *Nat. Chem.* **2010**, *2*, 329−334.
(5) Shichibu, Y.; Negishi, Y.; Tsunoyama, H.; Kanehara, M.; Teranishi, T.; Tsukuda, T. *Small* **2007**, *3*, 835−839.
(6) Beek, W. J. E.; Wienk, M. M.; Janssen, R. A. J. *Adv. Mater.* **2004**, *16*, 1009−1013.
(7) Caldwell, M. A.; Raoux, S.; Wang, R. Y.; Wong, H. S. P.; Milliron, D. *J. Mater. Chem.* **2010**, *20*, 1285−1291.
(8) Kelly, K. L.; Coronado, E.; Zhao, L. L.; Schatz, G. C. *J. Phys. Chem. B* **2003**, *107*, 668−677.
(9) Peng, P.; Milliron, D. J.; Hughes, S. M.; Johnson, J. C.; Alivisatos, A. P.; Saykally, R. J. *Nano Lett.* **2005**, *5*, 1809−1813.
(10) Biswas, S.; Belfield, K. D.; Das, R. K.; Ghosh, S.; Hebard, A. F. *Chem. Mater.* **2009**, *21*, 5644−5653.
(11) Papaefthymiou, G. C. *Nano Today* **2009**, *4*, 438−447.
(12) Chung, T.-H.; Wu, S.-H.; Yao, M.; Lu, C.-W.; Lin, Y.-S.; Hung, Y.; Mou, C.-Y.; Chen, Y.; Huang, D.-M. *Biomaterials* **2007**, *28*, 2959−2966.
(13) AshaRani, P. V.; Mun, G. L. K.; Hande, M. P.; Valiyaveetti, S. *ACS Nano* **2009**, *3*, 279−290.
(14) Zhang, Y.; Yang, M.; Park, J.-H.; Singelyn, J.; Ma, H.; Sailor, M. J.; Ruoslahti, E.; Ozkan, M.; Ozkan, C. *Small* **2009**, *5*, 1990−1996.
(15) Lin, C.-A. J.; Yang, T.-Y.; Lee, C. H.; Huang, S. H.; Sperling, R. A.; Zanella, M.; Li, J. K.; Shen, J.-L.; Wang, H. H.; Yeh, H.-I.; Parak, W. J.; Chang, W. H. *ACS Nano* **2009**, *3*, 395−401.
(16) Ackerson, C. J.; Jadzinsky, P. D.; Sexton, J. Z.; Bushnell, D. A.; Kornberg, R. D. *Bioconjugate Chem.* **2010**, *21*, 214−218.
(17) Bowman, M. C.; Ballard, T. E.; Ackerson, C. J.; Feldheim, D. L.; Margolis, D. M.; Melander, C. *J. Am. Chem. Soc.* **2008**, *130*, 6896−6897.
(18) Chen, R.; Ratnikova, T. A.; Stone, M. B.; Lin, S.; Lard, M.; Huang, G.; Hudson, J. A. S.; Ke, P. C. *Small* **2010**, *6*, 612−617.
(19) Cho, E. C.; Xie, J.; Wurm, P. A.; Xia, Y. *Nano Lett.* **2009**, *9*, 1080−1084.
(20) Cho, E. C.; Au, L.; Zhang, Q.; Xia, Y. *Small* **2009**, *6*, 517−522.
(21) Kim, C.; Agasti, S. S.; Zhu, Z.; Isaacs, L.; Rotello, V. M. *Nat. Chem.* **2010**, *2*, 962−966.
(22) Bresee, J.; Maier, K. E.; Boncella, A. E.; Melander, C.; Feldheim, D. L. *Small* **2011**, *7*, 2027−2031.
(23) Verma, A.; Uzun, O.; Hu, Y.; Hu, Y.; Han, H.-S.; Watson, N.; Chen, S.; D.J., I.; Stellacci, F. *Nat. Mater.* **2008**, *7*, 588−595.
(24) Leroueil, P. R.; Berry, S. A.; Duthie, K.; Han, G.; Rotello, V. M.; McNerny, D. Q.; Baker, J. R., Jr.; Orr, B. G.; Banaszak Holl, M. M. *Nano Lett.* **2008**, *8*, 420−424.
(25) Verma, A.; Stellacci, F. *Small* **2010**, *6*, 12−21.
(26) Chithrani, B. D.; Ghazani, A. A.; Chan, W. C. W. *Nano Lett.* **2006**, *6*, 662−668.
(27) Roiter, Y.; Ornatska, M.; Rammohan, A. R.; Balakrishnan, J.; Heine, D. R.; Minko, S. *Nano Lett.* **2008**, *8*, 941−944.
(28) Lin, J.; Zhang, H.; Chen, Z.; Zheng, Y. *ACS Nano* **2010**, *4*, 5421−5429.
(29) Yang, A.-C.; Weng, C.-J. *J. Chem. Phys.* **2010**, *114*, 8697−8709.
(30) Zhang, S.; Lykotrafitis, G.; Bao, G.; Suresh, S. *Adv. Mater.* **2009**, *21*, 419−424.
(31) Lin, J.-Q.; Zheng, Y.-G.; Zhang, H.-W.; Chen, Z. *Langmuir* **2011**, *27*, 8323−8332.
(32) Gurtovenko, A. A.; Anwar, J.; Vattulainen, I. *Chem. Rev.* **2010**, *110*, 6077−6103.
(33) Gurtovenko, A. A.; Vattulainen, I. *J. Am. Chem. Soc.* **2007**, *129*, 5358−5359.
(34) Gurtovenko, A. A.; Vattulainen, I. *J. Phys. Chem. B* **2008**, *112*, 4629−4634.
(35) Vácha, R.; Berkowitz, M.; Jungwirth, P. *Biophys. J.* **2009**, *96*, 4493−4501.
(36) Gurtovenko, A. A. *J. Chem. Phys.* **2005**, *122*, 244902.
(37) Lee, S. J.; Song, Y.; Baker, N. A. *Biophys. J.* **2008**, *94*, 3565−3576.
(38) Gurtovenko, A. A.; Vattulainen, I. *J. Phys. Chem. B* **2009**, *113*, 7194−7198.
(39) Arvizo, R. R.; Miranda, O. R.; Thompson, M. A.; Pabelick, C. M.; Bhattacharya, R.; Robertson, J. D.; Rotello, V. M.; Prakash, Y. S.; Mukherjee, P. *Nano Lett.* **2010**, *10*, 2543−2548.
(40) Salonen, E.; Lin, S.; Reid, M. L.; Allegood, M. S.; Wang, X.; Rao, A. M.; Vattulainen, I.; Ke, P. C. *Small* **2008**, *4*, 1986−1992.
(41) Milano, G.; Santangelo, G.; Ragone, F.; Cavallo, L.; Di Matteo, A. *J. Phys. Chem. C* **2011**, *115*, 15154−15163.
(42) Monticelli, L.; Salonen, E.; Ke, P. C.; Vattulainen, I. *Soft Matter* **2009**, *5*, 4433−4445.
(43) Chaki, N.; Negishi, Y.; Tsunoyama, H.; Shichibu, Y.; Tsukuda, T. *J. Am. Chem. Soc.* **2008**, *130*, 8608−8610.
(44) Qian, H.; Jin, R. *Nano Lett.* **2009**, *9*, 4083−4087.
(45) Fields-Zinna, C. A.; Sardar, R.; Beasley, C. A.; Murray, R. W. *J. Am. Chem. Soc.* **2009**, *131*, 16266−16271.
(46) Qian, H.; Jin, R. *Chem. Mater.* **2011**, *23*, 2209−2217.
(47) Jadzinsky, P. D.; Calero, G.; Ackerson, C. J.; Bushnell, D. A.; Kornberg, R. D. *Science* **2007**, *318*, 430−433.
(48) Heaven, M. W.; Dass, A.; White, P. S.; Holt, K. M.; Murray, R. W. *J. Am. Chem. Soc.* **2008**, *130*, 3754−3755.
(49) Akola, J.; Walter, M.; Whetten, R.; Häkkinen, H.; Grönbeck, H. *J. Am. Chem. Soc.* **2008**, *130*, 3756−3757.
(50) Qian, H.; Eckenhoff, W.; Zhu, Y.; Pintauer, T.; Jin, R. *J. Am. Chem. Soc.* **2010**, *132*, 8280−8281.
(51) Lopez-Acevedo, O.; Akola, J.; Whetten, R.; Grönbeck, H.; Häkkinen, H. *J. Phys. Chem. C* **2009**, *113*, 5035−5038.
(52) Schaaff, T. G.; Shafigullin, M. N.; Khoury, J. T.; Vezmar, I.; Whetten, R. L. *J. Phys. Chem. B* **2001**, *105*, 8785−8796.
(53) Hicks, J. F.; Miles, D. T.; Murray, R. W. *J. Am. Chem. Soc.* **2002**, *124*, 13322−13328.

(54) Laaksonen, T.; Ruiz, V.; Liljeroth, P.; Quinn, B. M. *Chem. Soc. Rev.* **2008**, *37*, 1836−1846.
(55) Berendsen, H. J. C.; van der Spoel, D.; van Drunen, R. *Comput. Phys. Commun.* **1995**, *91*, 43−56.
(56) Tieleman, D. P.; Berendsen, H. J. C. *Biophys. J.* **1998**, *74*, 2786−2801.
(57) Mukhopadhyay, P.; Monticelli, L.; Tieleman, D. P. *Biophys. J.* **2004**, *86*, 1601−1609.
(58) Heinz, H.; Vaia, R. A.; Farmer, B. L.; Naik, R. R. *J. Phys. Chem. B* **2008**, *112*, 17281−17290.
(59) Berendsen, H. J. C.; Postma, J. P. M.; van Gunsteren, W. F.; Hermans, J. In *Intermolecular Forces*; Pullman, B., Ed.; Reidel: Dordrecht, The Netherlands, 1981; Chapter Interaction models for water in relation to protein hydration.
(60) Essmann, U. L.; Perera, L.; Berkowitz, M. L.; Darden, T.; Lee, H.; Pedersen, L. G. A. *J. Chem. Phys.* **1995**, *103*, 8577−8593.
(61) Van Der Spoel, D.; Lindahl, E.; Hess, B.; Groenhof, G.; Mark, A. E.; Berendsen, H. J. C. *J. Comput. Chem.* **2005**, *26*, 1701−1718.
(62) Berendsen, H. J. C.; Postma, J. P. M; Van Gunsteren, W. F.; Dinola, A.; Haak, J. R. *J. Chem. Phys.* **1984**, *81*, 3684−3690.
(63) Van der Spoel, D.; Van Maaren, P.; Larsson, P.; Tîmneanu, N. *J. Phys. Chem. B* **2006**, *110*, 4393−4398.
(64) Chaikin, P.; Lubensky, T. *Principles of Condensed Matter Physics*; Cambridge University Press: Cambridge, U.K., 1995.
(65) Gurtovenko, A. A.; Patra, M.; Karttunen, M.; Vattulainen, I. *Biophys. J.* **2004**, *86*, 3461−3472.
(66) Sammalkorpi, M.; Karttunen, M.; Haataja, M. *J. Phys. Chem. B* **2009**, *113*, 5863−5870.
(67) Mark, P.; Nilsson, L. *J. Phys. Chem. A* **2001**, *105*, 9954−9960.
(68) Gurtovenko, A. A.; Vattulainen, I. *J. Phys. Chem. B* **2008**, *112*, 1953−1962.